



Lawrence Berkeley Laboratory

UNIVERSITY OF CALIFORNIA

ENERGY & ENVIRONMENT DIVISION

To be presented at the 1981 Fall Meeting, Western States Section/The Combustion Institute, Tempe, AZ, October 19-20, 1981

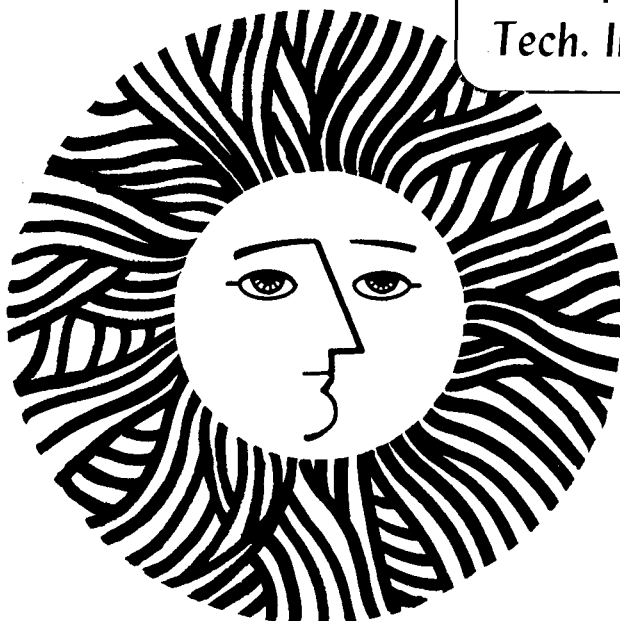
VELOCITY STATISTICS IN PREMIXED TURBULENT FLAME

R.K. Cheng and T.T. Ng

October 1981

TWO-WEEK LOAN COPY

This is a Library Circulating Copy which may be borrowed for two weeks. For a personal retention copy, call Tech. Info. Division, Ext. 6782



RECEIVED
BERKELEY LABORATORY

OCT 21 1981

LIBRARY AND
DOCUMENTS SECTION

LBL-13367
c-2

DISCLAIMER

This document was prepared as an account of work sponsored by the United States Government. While this document is believed to contain correct information, neither the United States Government nor any agency thereof, nor the Regents of the University of California, nor any of their employees, makes any warranty, express or implied, or assumes any legal responsibility for the accuracy, completeness, or usefulness of any information, apparatus, product, or process disclosed, or represents that its use would not infringe privately owned rights. Reference herein to any specific commercial product, process, or service by its trade name, trademark, manufacturer, or otherwise, does not necessarily constitute or imply its endorsement, recommendation, or favoring by the United States Government or any agency thereof, or the Regents of the University of California. The views and opinions of authors expressed herein do not necessarily state or reflect those of the United States Government or any agency thereof or the Regents of the University of California.

VELOCITY STATISTICS IN PREMIXED TURBULENT FLAME

by

R. K. Cheng and T. T. Ng

Lawrence Berkeley Laboratory
University of California
Berkeley, California 94720

Velocity statistics in unconfined, V-shaped, premixed ethylene/air flames propagating in grid or perforated plate induced turbulence were studied using laser Doppler velocimetry. These data were interpreted with reference to schlieren records showing the shape and orientation of the instantaneous flame sheets. Mean profiles of two velocity components, their rms fluctuation levels and Reynolds stress at several axial cross sections were obtained. Probability density functions, spectral density distributions and streamwise macroscale profiles through the flame were also deduced. Peak rms fluctuations in the flame region were found to depend on the shape, size and orientation of the flame convolutions. An increase in Reynolds stress inside the flame region was observed. The apparent high turbulence production seemed to be an effect of the fluctuating flame sheet moving about the stationary LDV probe, but not intrinsic to fluid mechanical turbulence production.

This work was supported by the Director, Office of Energy Research, Office of Basic Energy Sciences, Chemical Sciences Division of the U. S. Department of Energy under contract No. W-7405-ENG-48.

This manuscript was printed from originals provided by the authors.

1. INTRODUCTION

Although considerable progress has been made in the study of pre-mixed turbulent flame propagation by recent experimental and theoretical investigations,¹⁻⁷ many aspects of the interaction between turbulence and combustion are not yet fully understood. More experimental data are needed to further quantify the effects of turbulence level and associated length scales on flame propagation, and to verify the concept of 'flame generated' turbulence and Reynolds stress predicted by turbulent flame models.¹

With the development of laser based diagnostics techniques most experimental investigations are now concentrated on detailed statistical measurements of scalar and velocity fluctuations and their cross-correlation parameters. Yoshida³ measured temperature and two velocity component statistics in a Bunsen type premixed flame with low intensity incident turbulence and reported no change in turbulence fluctuations and Reynolds stress in the flame region. Yanigi and Mimura⁴ focussed their efforts on obtaining velocity and temperature cross-correlations also in a Bunsen type premixed turbulent flame. They reported radial counter gradient turbulent heat transfer phenomena which could only be explained by the fluctuating laminar flame structures. Dandekar and Gouldin⁵ studied turbulent flame speed in a premixed, rod-stabilized v-shaped flame in grid-induced turbulence and reported turbulence length scales and statistical measurements of two velocity components. Their results show a significant increase in root-mean-square (rms) velocity fluctuations in the flame region which seemed to influence turbulent flame speed. Bill et. al.⁵ measured density and streamwise velocity

statistics in a similar flame. Significant increase in velocity fluctuations was observed except in a lean flame with highly oblique flame angle. Subsequent study of Cheng and Ng⁷ indicated deflections of the streamlines in the entire flow-field and an increase in incident turbulence level upstream from the flame. The influence of the flame stabilizer wake on flame propagation was also found to be significant in many situations.

As demonstrated by these results, statistical data obtained in premixed turbulent flame are not very consistent and seem to depend on the burner type and flame geometry. Interpretation of these data is difficult because both the effects of high heat release and velocity gradients induced by the flame fronts have to be considered. Very often, the instantaneous flame structures based on wrinkled laminar flame model assumptions were used in order to explain the irregular statistical behavior.⁴

Knowledge of the detail flame structures and the overall flame characteristics seem to be the key to facilitate the interpretation of statistical data. The objective of the present study is to combine qualitative information inferred from schlieren records with quantitative velocity data obtained from laser Doppler velocimetry (LDV) measurements to study the propagation of premixed turbulent flames.

The flame configuration is a v-shaped premixed ethylene/air flame stabilized in turbulence generated by a grid or perforated plates. Two components of mean and rms velocities and the Reynolds stress were obtained from single-component LDV measurements. In addition, the streamwise macroscale, the probability density functions, and the

streamwise velocity spectral density distributions were also deduced.

2. EXPERIMENTAL ARRANGEMENTS

The v-shaped flame was stabilized in an unconfined circular coaxial jet with inner core of ethylene/air mixture 2.5 cm in diameter surrounded by air of 5.0 cm outer diameter. Figure 1 is a schematic of half of the flame plane depicting the orientations of the co-ordinate system and velocity components measured in this study. Turbulence in the jet was generated by turbulence generators placed 50 mm upstream of the 1.0 mm diameter flame stabilizer rod. Three different turbulence generators were used: a bi-plane grid with mesh size, M , of 5.0 mm with 1.0 mm elements, and two perforated plates - #1 with 3.2 mm circular holes 1.6 mm apart and #2 with 4.76 mm circular holes 1.8 mm apart.

Flame propagation in grid-induced turbulence was studied for four conditions with free-stream velocity, U_{∞} , at 5.0 and 7.0 m/s and equivalence ratios, ϕ , ranging from 0.66 to 0.8. Flame propagation in turbulence generated by the two perforated plates was studied for $U_{\infty} = 7.0$ m/s and $\phi = 0.75$.

A Spectra Physics 4 watt argon ion laser was used as the light source for schlieren photography and LDV. The schlieren optics consisted of a pair of 1000 mm focal length lenses and a polarization prism schlieren stop.⁸ The still schlieren photographs were taken with a 4" by 5" frame camera, and the high speed schlieren movies were taken with a Fastax camera with framing rate up to 4 kHz.

The LDV optics consisted of a 5 cm fixed separation beam splitter,

and a 250 mm focal length lens to form the scattering volume. Aluminum oxide particles of 0.3 μm were introduced by a cyclone canister type seeder. Scattered Doppler bursts were collected at forward direction using a lens, filter and photomultiplier assembly. The signals were processed with a TSI 1090 counter unit which was interfaced with a computer controlled data acquisition system based on a PDP 11/10 mini-computer. Further details of the data acquisition system were described in ref. 6.

The procedure to deduce mean streamwise and cross-stream velocity, U and V respectively, and their rms fluctuations, u' and v' and the Reynolds stress, $-\overline{uv}$, from measurements of three velocity components U , U_1 and U_2 was described in detail by Duranni and Greated.⁹ For our study, the three components were oriented at 0° and $\pm 30^\circ$ with respect to the x-axis. Typical data rates ranged from about 10 kHz in the free stream to 3.5 kHz inside the hot region. Due to these high data rates, it was possible to process the analog output of the counter as continuous. The flame was scanned automatically at 30 preselected traverse positions where 8192 samples were digitized at a rate of 2.5 kHz. Profiles at six axial locations were obtained for each experimental condition to cover the whole flow-field. Progress of the experiment was monitored by plotting mean velocity data graphically on a video terminal. Raw data were stored on 7 tracks magnetic tapes for post processing at the Lawrence Berkeley Laboratory CDC 7600 computer.

The probability density functions (pdf) of the three components were based on the histogram of the velocity time series using 40

windows. Using Taylor's hypothesis, the streamwise macroscale, l_x , was obtained from the product of the local streamwise velocity and the integral time scale, τ_x .

$$l_x = U \cdot \tau_x \quad (1)$$

The integral time scale was obtained by integrating and normalizing the area between the auto-correlation function, $f(t)$, and its asymptotic value, $f(a)$, as :

$$\tau_x = \frac{1}{1-f(a)} \int_0^{\infty} (f(t) - f(a)) dt \quad (2)$$

The velocity spectral density distributions were calculated by the Fast Fourier Transform (FFT) algorithm. To reduce the error in the spectral density distributions which is proportional to the number of spectral records used for the averaging, the data time series were grouped to obtain 64 spectral records.

3. RESULTS

3.1 Incident Turbulence

Turbulence generated by the three turbulence generators is compared in Fig. 2. on the (U_{∞}^2/u'^2) vs. (x/M) plane, developed by Batchelor and Twonson¹⁰ for isentropic turbulence. As demonstrated in our earlier works,^{6,7} turbulence produced by the grid is linear on this plane; the data in Fig. 2 give a slope of 68. The data for the two perforated

plates also show a linear decay with x , but their decay rates are much lower than that of the grid. The slopes of the lines in Fig. 2 are 16 for plate #1 and 22 for plate #2.

Fluctuation intensities generated by the perforated plates are not significantly higher than the 5% turbulence generated by the grid. With freestream velocity of 7.0 m/s, plate #1 generates $u' = 7.0\%$ and $v' = 5.5\%$, plate #2 generates $u' = 8.5\%$ and $v' = 7.5\%$, all measured at $x = 60$ mm. Since in both cases u' is higher than v' , the turbulence is not isentropic.

At $x = 60$ mm, streamwise macroscale for the grid averaged approximately 5.0 mm, which is within the range $2.0 < l_x < 6.0$ mm predicted by isentropic turbulence analysis for this condition. Values of l_x for the perforated plates were 4.0 mm for plate #1 and 3.5 mm for plate #2. In all three cases, l_x increases downstream as the turbulence decays. The growth rates of the macroscales were linear with x up to $x = 100$ mm.

3.2 Mean Velocities and Flame Structures

A typical set of mean velocity profiles is shown in Fig. 3 for the condition of $U_\infty = 5.0$ m/s and $\phi = 0.8$. The acceleration of flow velocity through the flame region is more pronounced on the cross-stream component. Therefore the cross-stream velocity profiles are more appropriate for deducing the mean flame positions. Since there is no standard definition of mean flame position in a turbulent flame based on velocity measurements, we define it as the position of maximum cross-stream velocity gradient, $(dV/dy)_{\max}$. In Fig. 3, this

corresponds to $x = 6.5$ mm, a position close to where V crosses zero. It is interesting to note that the maximum streamwise velocity gradient also occurs near there, although the local U is only slightly higher than U_{∞} .

A convenient means of illustrating some overall features of the flame is by plotting the two-dimensional velocity vector field. The vector fields for all experimental conditions using the grid were included in our previous paper.⁷ Shown in Fig. 4 are the velocity vector fields of three flames with identical initial condition of $U_{\infty} = 7.0$ m/s and $\phi = 0.75$ but using different turbulence generators. The mean flame positions and the cold boundary of the flame region are also shown to compare the extent of flame spread. The cold boundary is defined here as the point where V increases from its free-stream level.

The most prominent effect of the higher turbulence intensity produced by the perforated plates is to augment the size of the flame region. However, the size of the flame region does not seem to be directly proportional to turbulence intensity for the flame region using plate #1 (Fig. 4(b)) is slightly larger than that using plate #2 (Fig. 4(c)), though the turbulence produced by plate #1 is lower. Although the mean flame positions of the three flames are not coincidental, the local flame angles are not significantly different. Flow deflections in the free stream up to $x = 80$ mm are also quite similar, which confirms our earlier conclusion that the flow deflection angle is essentially proportional to the flame angle.

Some characteristic features of the two flames using the grid and plate #1 (Figs. 4(a) and 4(c)) are shown on the schlieren records in

Fig. 5. Since the optical axis was arranged parallel to the flame stabilizer, the schlieren images were the result of incident light passing through several convoluted flame fronts on the flame sheet. Consequently, many details of the flame convolutions were obliterated. Nevertheless, one interesting feature is demonstrated on both records: the occasional flaring of flame pockets into the freestream, as indicated by the arrows on the right side of the flames.

To show more structural details of the flame sheet, schlieren records were taken of inverted conical flames, stabilized by a blunt body under the same conditions as the V-shaped flames of Fig. 5. These records (Fig. 6) show the main differences between the flames in grid and perforated induced turbulence to be the size, number density and orientation of the flame convolutions. In the flame of Fig. 6(a), associated with the grid, the flame sheet remains quite smooth for a distance downstream from the flame stabilizer. Slight wrinkling of the flame sheet then develops and amplifies into round flame convolutions. High-speed schlieren movies of this flame show that the flame convolutions are convected along the surface of the flame sheet at rather constant phase velocities. In contrast to the flame of Fig. 6(a), the wrinkling of the flame sheet of Fig. 6(b) associated with plate #1 occurs almost immediately downstream of the flame stabilizer. The subsequent flame convolutions are smaller and more elongated than those of Fig. 6(a) and the flame cusps where the convex convolutions meet are deeper and sharper. The flame sheet is so highly convoluted that many of the convolutions develop apexes pointing upstream, as indicated by the arrows on the left side of Fig. 5(b) and Fig. 6(b).

It is possible that some of these flame convolutions may detach from the flame sheet, resulting in the flaring mentioned earlier. Since the flaring seems closely associated with the degree of flame convolutions, it occurs only near the top of the flame in grid induced turbulence. In perforated plate induced turbulence, the flame convolution are developed more rapidly, so flaring occurs closer to the stabilizer rod.

Although the turbulence intensities and length scales produced by the grid and the perforated plates are not significantly different, the features shown on the schlieren records are quite dissimilar. These qualitative features of the flame sheet are used in the next section to interpret the quantitative statistical measurements.

3.3 Velocity Statistics

3.3-1 RMS Fluctuations

The rms fluctuation profiles at $x = 60, 80,$ and 100 mm for the condition of $U_{\infty} = 7.0$ m/s and $\phi = 0.75$ (Fig. 4(a)) are shown in Fig. 7. In the free stream, the streamwise and cross-stream fluctuation levels are both at about 5% agreeing with the isentropic turbulence assumption for grid induced turbulence. At $x = 60$ mm, where the flame is at $y = 2.5$ mm, the fluctuations do not show any change through the flame region. Rather, u' increases to about 8% at $y = 0$, showing the influence of the flame stabilizer wake on flame propagation at this axial location. Fluctuation profiles with these features were observed throughout the flow field of the flame with $U_{\infty} = 7.0$ m/s $\phi = 0.6$. Under this lean condition, the mean flame angle was very oblique and the wake was found to dominate flame propagation up to $x = 100$ mm.

At $x = 80$ and 100 mm where the flame stabilizer wake becomes less predominant, both u' and v' increase sharply inside the flame region. This increase in fluctuation level is primarily due to the flame fronts passing through the stationary LDV probe. It is interesting to note that a trace of the flame stabilizer wake is still visible at $x = 80$ mm near $y = 0$. In the hot region, fluctuations are slightly less than the incident turbulence, indicating that turbulence kinetic energy is not increased by combustion heat release.

In all of the flame studied, the peak fluctuation intensities are found to increase with increasing x , and are located at different positions inside the flame region. The u' peaks are skewed to the boundary of the hot region and the v' peaks are skewed to the boundary of the cold region. For conditions using the grid, as in Fig. 7, the v' peaks are substantially higher than the u' peaks. The largest difference in fluctuation intensities is found for $U_\infty = 5.0$ m/s and $\phi = 0.8$, a condition of increased heat release rates, where it exceeds 10%. Fluctuation profiles in the flames propagating in perforated plate induced turbulence do not show this difference in peak intensities. As demonstrated in Fig. 8, which shows a typical set of fluctuation profiles in the flame of Fig. 4(b), the peak fluctuation intensities are about equal. These different features of the fluctuation profiles can be explained by the structures of the flame sheets in the grid and the perforated plate induced turbulence.

The locations of the u' and v' peaks are associated with the locations of the flame convolutions and flame cusps. The flame convolutions are convex towards the cold region, the instantaneous flame fronts

of the convex part of the convolutions, which are oblique to the x-axis, occupy the region near the cold reactants. Acceleration due to combustion heat release through these flame fronts induces fluctuations primarily in the cross-stream direction, resulting in a v' peak near the cold boundary of the flame region. On the other hand, the flame cusps are located near the hot region and their flame fronts are more oblique to the y-axis, therefore the streamwise fluctuation induced by flame cusps peaks near the hot region.

The difference in peak fluctuation intensities can be explained by the orientation of the instantaneous flame fronts. In grid induced turbulence, the flame is characterized by large convolutions with shallow cusps. The instantaneous flame fronts are mostly oriented parallel to the mean flame orientation, inducing fluctuations primarily in the cross-stream direction. In perforated plate induced turbulence, the instantaneous flame fronts in the highly convoluted flame sheet and the deep, sharp flame cusps have no preferred orientation. Hence, the streamwise and cross-stream fluctuations are comparable.

3.3-2 Reynolds Stress

The Reynolds stress profiles corresponding to the data of Fig. 7 are shown in Fig. 9. As predicted for grid induced turbulence, the Reynolds stress in the free-stream is negligible. At $x = 60$ mm, the profiles remain unchanged through the flame region. The slight increase near $y = 0$ is due to the flame stabilizer wake. At $x = 80$ and 100 mm, the Reynolds stress increases inside the flame region but drops back to zero in the hot region. The peak Reynolds stresses are found to

increase with increasing x , and are located between the positions of maximum u' and v' .

The Reynolds stress inside the flame seems to be caused by the flame fronts passing through the LDV probe and may not be related to fluid mechanical turbulence production. As demonstrated in Fig. 10, showing the velocity vectors of a fluid element before and after its encounter with an instantaneous flame front, the velocity component orthogonal to the flame orientation is accelerated due to fluid expansion while the tangential component remains unchanged. When this occurs, the flow direction is changed from outward to inward. This is consistent with the mean velocity vector fields. It follows that the flow in the flame region as seen by the LDV probe consists mainly of slow outward-moving reactants interfaced with fast inward-moving products. The cross-correlation between u and v is always negative because in the reactants, u is negative and v is positive whereas in the products their signs are reversed. The absolute value of the cross-correlation increase proportionally to the probability of flame front passage, peaking at where the passage of a flame front is most frequent. Although the rms fluctuations in the flame region are also related to the probability of flame front passage, due to the difference in the flame front orientation mentioned earlier, their peaks are on either side of this positions.

The coefficient of correlation ($-\overline{uv}/u'v'$) between the velocity fluctuations, u and v , is shown in fig. 11. In the flame region, velocity fluctuations induced by the flame fronts are superimposed on the random incident turbulence. At $x = 80$ mm,

where the increase in fluctuations due to the flame is not very significant, the peak value of the coefficient is about 0.55. However, at $x = 100$ mm, where the flame induced fluctuations are more appreciable, peak value of the coefficient increases to 0.75. The peak values at $x = 100$ mm obtained from the other experimental conditions using the grid and the perforated plates vary from 0.7 to 0.9. It is of interest to note that if the variance of the incident turbulence were subtracted from the variance of the fluctuations in the flame region and use as a measure of the flame induced fluctuation to obtain the coefficient of correlation, the peak values would increase to about 0.8 to 0.95 at all axial locations. This result is of significance because it demonstrates that the high Reynolds stress is a consequence of the flame induced fluctuations. Since the turbulent kinetic energy in the hot region is not increased, the apparent high turbulence production in the flame region as indicated by the increase in Reynolds stress does not seem to be intrinsic to fluid mechanical turbulence production.

3.3-3 Probability Density Function (pdf)

The influence of flame structures on turbulence statistics is further emphasized by the sets of pdf's in Fig. 12. The pdf's for the three velocity components are shown at the positions of maximum cross-stream velocity fluctuation. In Fig. 12(a), a highly bimodal distribution is shown for U_2 , the distribution for U is slightly bimodal, but for U_1 a single-peaked distribution is shown. These distributions are typical for a flame with instantaneous flame fronts mostly parallel to the mean flame angle. The effect of the flame fronts passing

through the LDV probe is most pronounced on the U_2 distribution, for this component is almost normal to the mean flame angle. The U component is oblique to the flame and its distribution is less affected. The U_1 component is almost parallel to the flame and therefore its pdf does not show the flame induced fluctuations.

In Fig. 12(b), the U_2 distribution is less bimodal, the U distribution shows a single-peaked distribution, and the U_1 distribution is unaffected. These distributions correspond to instantaneous flame fronts with more random orientations. In Fig. 12(c), the U_2 distribution is not bimodal but skewed towards the lower velocities. Note that the U and U_1 distributions are almost identical. These distributions are associated with a flame with no preferred flame front orientation.

3.3-4 Streamwise Macroscale and Spectral Density Distribution

A typical profile of streamwise macroscale, l_x , through a turbulent flame is shown in Fig. 13. The flame region, inferred from the mean cross-stream velocity profile, extends from $y = 6$ to 15 mm, and the mean flame position is at $y = 9$ mm. The flame does not seem to have a significant effect on the macroscale in the region close to the cold boundary but produces a dip near the mean flame position. A gradual increase in the macroscale is shown near the hot boundary of the flame region. At $y = 0$ the macroscale reached its maximum value of about 13 mm. The larger macroscale observed in the hot region suggest that the size of the turbulent eddies is enlarged by fluid expansion.

The enlargement of turbulent eddies by combustion heat release is

also shown on the streamwise spectral density distributions in the cold ($x = 16$ mm), hot ($x = 2.5$ mm) and flame ($x = 5.5$ mm) regions compared in Fig. 14. The increased velocity fluctuations in the flame region contributes primarily to frequencies below 300 Hz. These low frequencies are consistent with the rate at which flame fronts pass through the LDV probe. In the hot region, the distribution is identical to that of the incident turbulence up to 200 Hz, showing that the combustion heat release does not seem to alter the turbulence characteristics in the low frequencies. However, the distribution begins to deviate below the incident turbulence distribution in the high frequency range above 200 Hz, and levels out at about 1000 Hz.

As discussed earlier, the data rate inside the flame region was about 3.5 kHz, which was not significantly higher than the sampling rate of 2.5 kHz. Treating the counter output as continuous may have obliterated some of the high frequency fluctuations. However, deviation between the distributions in the cold and hot regions begins at a frequency range which should not be affected by this treatment. Therefore, the observed changes in macroscales and spectral density distributions are related to fluid mechanical phenomena and are not caused by the limitations of the diagnostics methods.

4. CONCLUSIONS

Premixed flame propagation in grid and perforated plate induced turbulence had been studied by the use of schlieren photography and laser Doppler velocimetry. The characteristic features of the flame sheets shown on the schlieren records were found to be quite useful

for the interpretation of the velocity statistical data. Under identical initial conditions, the size of the flame region in perforated plate induced turbulence is larger than that in grid induced turbulence because the flame convolutions are developed and amplified more rapidly in the former flow. However, the mean flame angle and free-stream flow deflections seems to be unaffected by the different incident turbulence.

Increases in both the streamwise and cross-stream rms velocity fluctuations are significant inside the flame region. This is caused by the movement of the flame fronts about the stationary LDV probe. The fluctuation intensities in the hot region are comparable to or less than that of the incident turbulence. The positions of the peak fluctuations seems to be associated with the locations of the convex flame convolutions and the flame cusps. The difference in the peak fluctuation intensities can be explained by whether the instantaneous flame fronts have any preferred orientation.

The increase in Reynolds stress inside the flame region is also significant and seems to be consistent with the change in flow direction induced by the fluctuating flame fronts. The high values of the coefficient of correlation further indicate that the Reynolds stress is a consequence of the flame induced fluctuations and may not be intrinsic to the fluid mechanical turbulence production.

The features of the pdf's inside the flame region are closely associated with the flame structures, emphasising the interrelation between the flame structures and the velocity statistics. The expansion of the turbulence eddies by combustion heat release is shown on both the profiles of macroscale and by the comparison of spectral density distributions.

ACKNOWLEDGEMENT

This work was supported by the Director, Office of Energy Research, Office of Basic Energy Sciences, Chemical Sciences Division of the U. S. Department of Energy under contract No. W-7405-ENG-48.

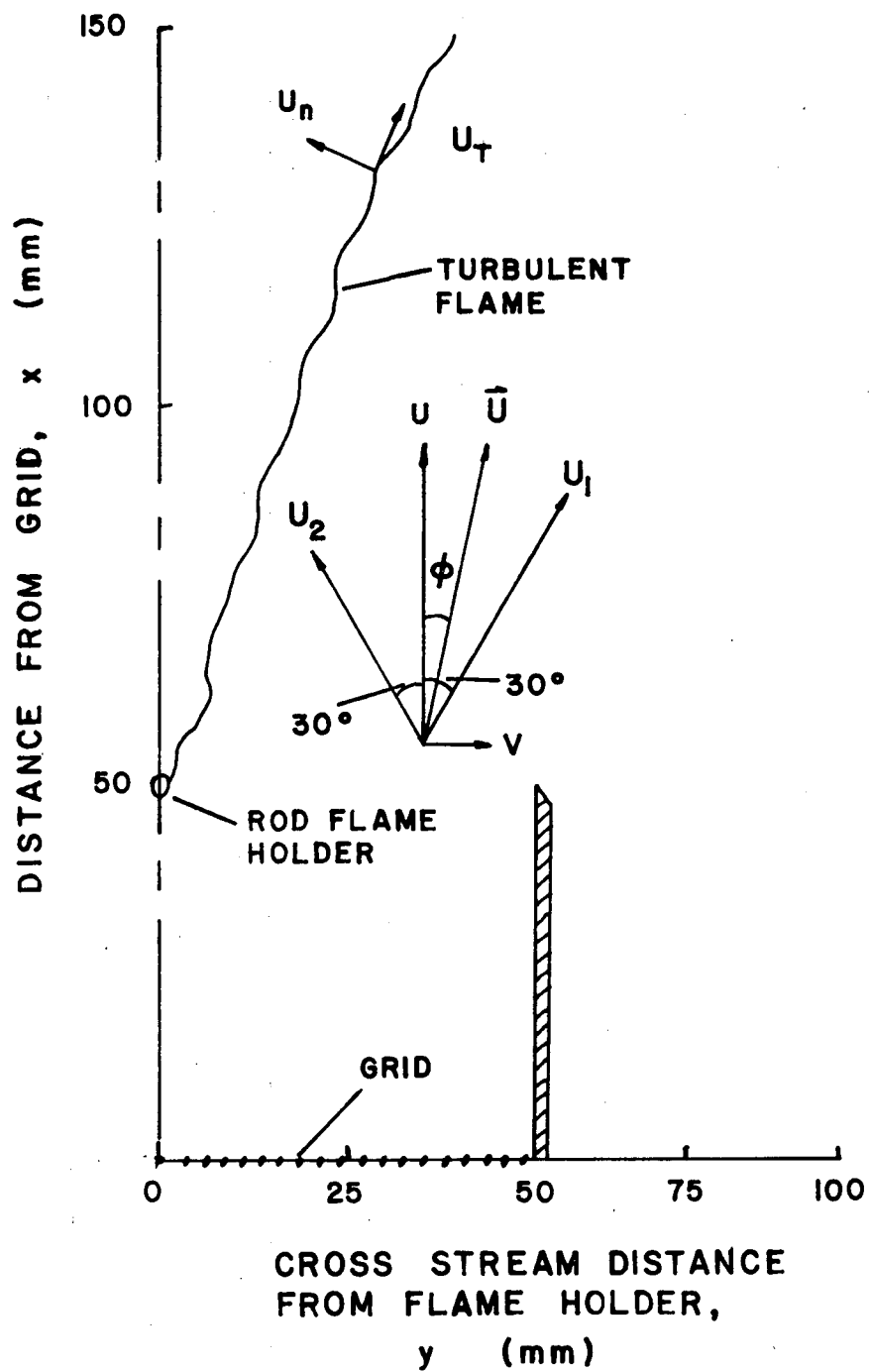
The authors would like to thank Dr. F. Robben and Prof. L. Talbot for their advise and support, and Mr. G. Douthwaite for his assistance in preparing the manuscript.

REFERENCES

1. Bray, K. N. C., Libby, P. A., and Masuya, G., First Specialist Meeting (International) of the Combustion Institute, The French Section of the Combustion Institute, 1,1, 1981.
2. Clavin, P., and Willians, F. A., J. Fluid Mech., 90, 3, 1979.
3. Yoshida, A., Eighteenth (Int'l) Symposium on Combustion, The Combustion Institute, 931, 1981.
4. Yanigi, T., and Mimura., Y., Eighteenth (Int'l) Symposium on Combustion, The Combustion Institute, 1031, 1981.
5. Dandekar, K. V., and Gouldin, F. C., AIAA 19th Aerospace Sciences Meeting, AIAA paper No. 81-0179, 1981.
6. Bill, R. G., Jr., Namer, I., Talbot, L., Cheng, R. K., and Robben, F., to be published in Combsution and Flame, 1981.
7. Cheng, R. K., and Ng, T. T., First Specialist Meeting (International) of the Combustion Institute, The French Section of the Combustion Insitute, 1, 13, 1981.
8. Oppenheim, A. K., Urtiew, P. A., and Weinberg, F. J., Proc. Roy. Soc.

(London), A291, 279, 1966.

9. Durrani, T. S., and Greated, C. A., Laser Systems in Flow Measurement, Plenum Press, New York, 1979.
10. Batchelor, G. K., and Townsend, A., Proc. Roy. Soc., A, 193, 539, 1948.



XBL 811-7540

Fig. 1 Schematics of the experimental setup.

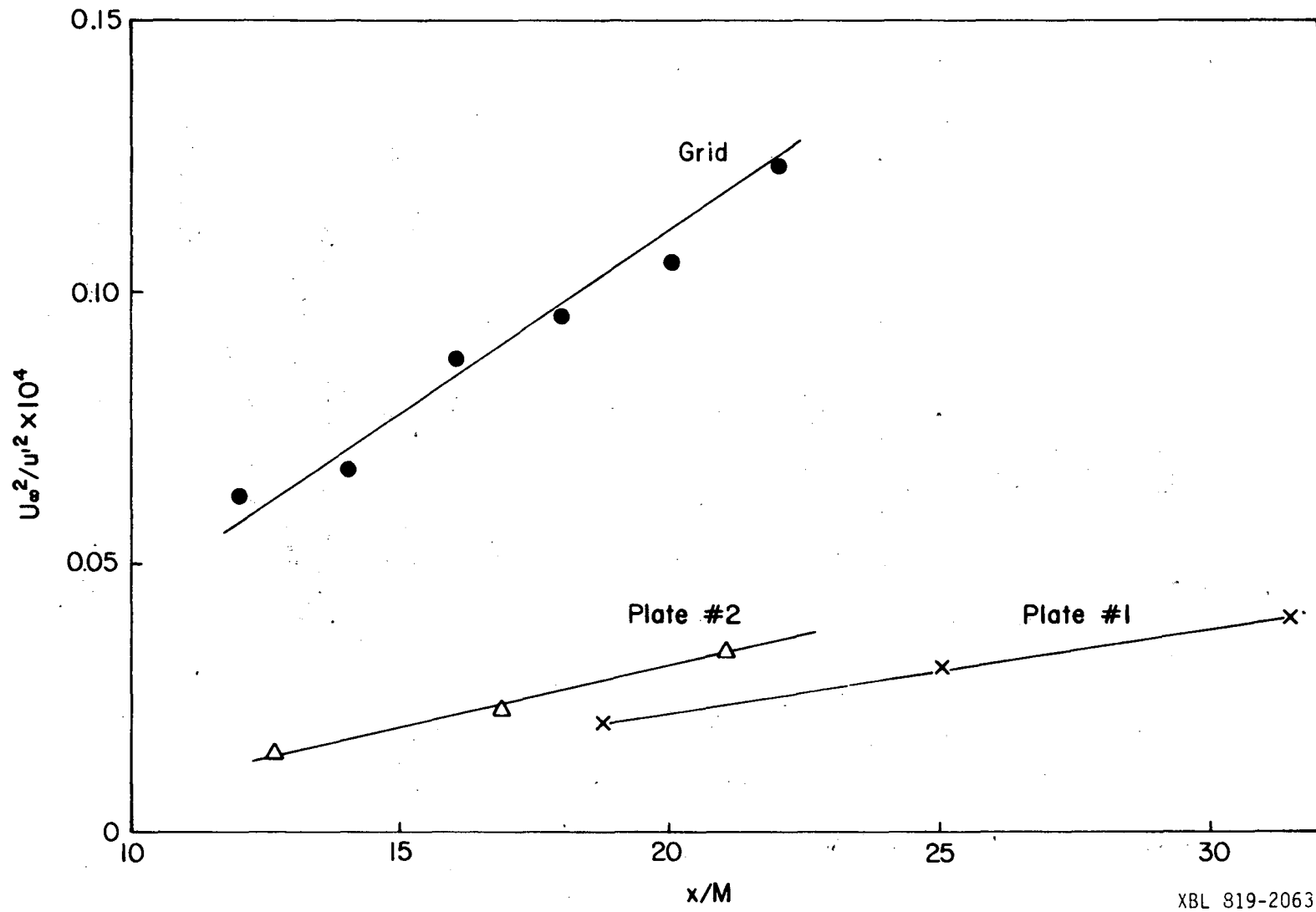
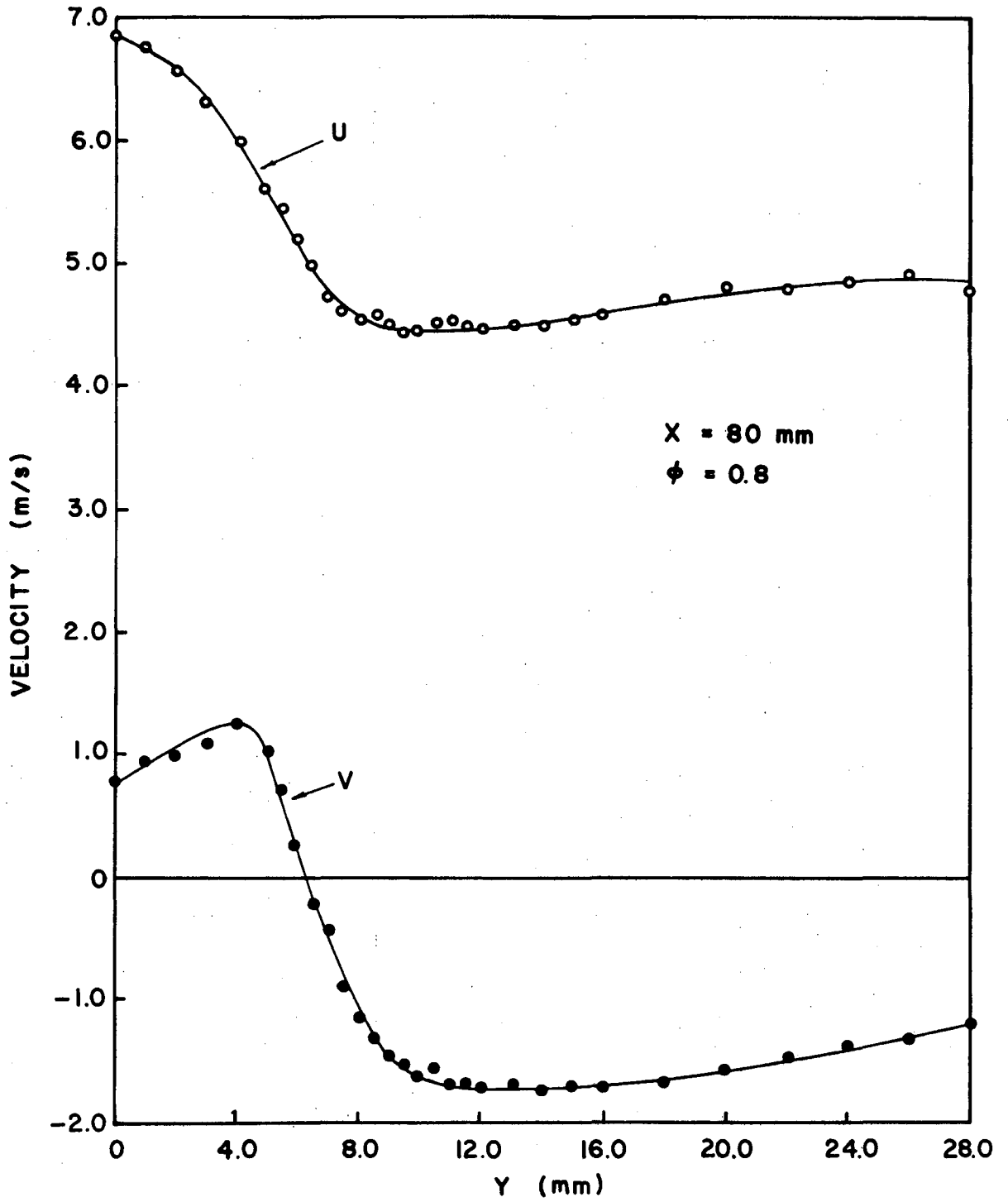
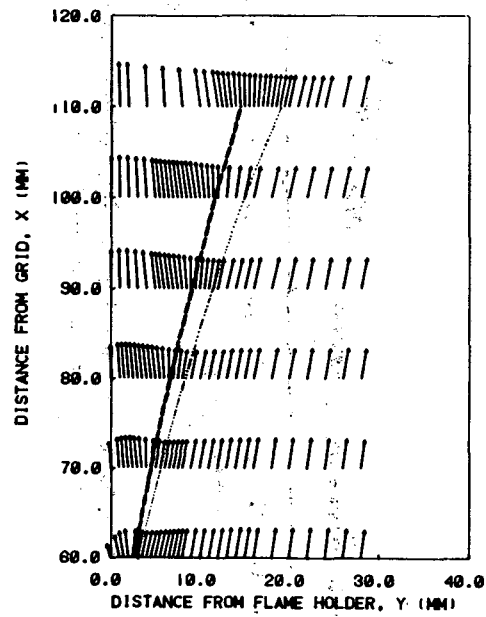


Fig. 2 Comparison of streamwise fluctuation levels produced by the three turbulence generators.

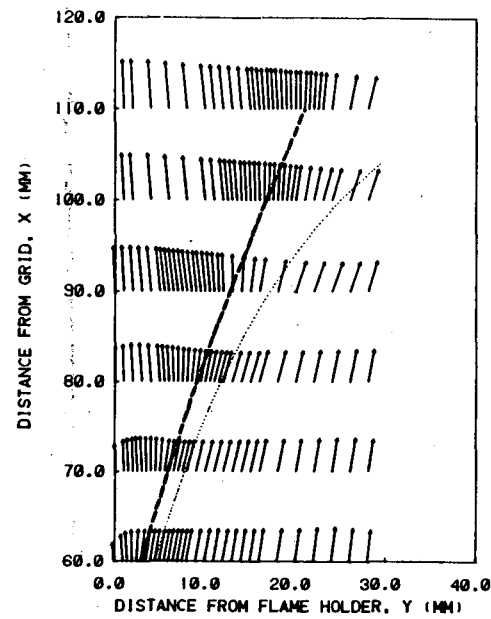


XBL 817-10641

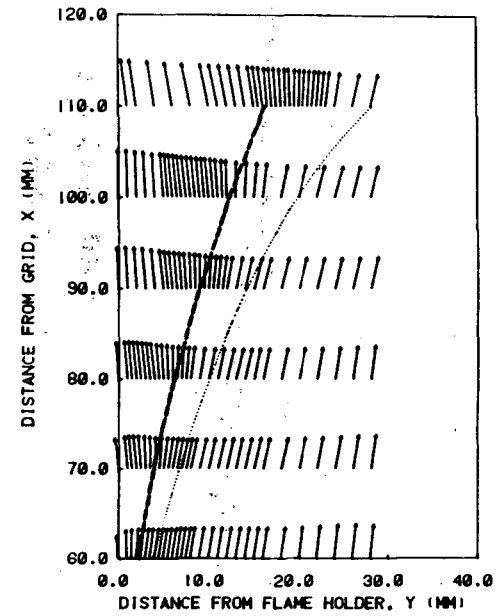
Fig. 3 Mean velocity profiles through a V-shaped turbulent flame; $U_{\infty} = 5.0$ m/s, $\phi = 0.8$, $x = 80.0$ mm.



(a)

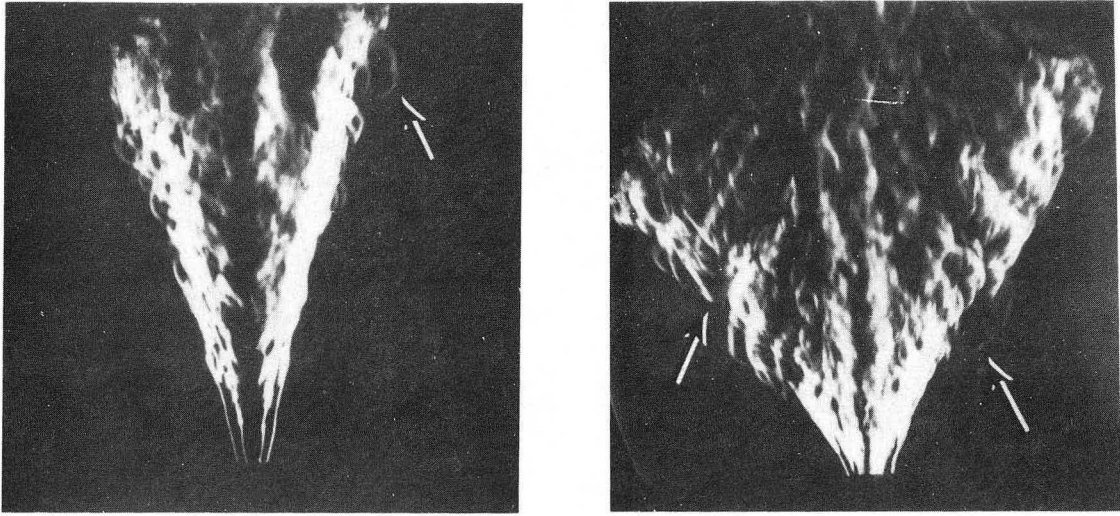


(b)



(c)

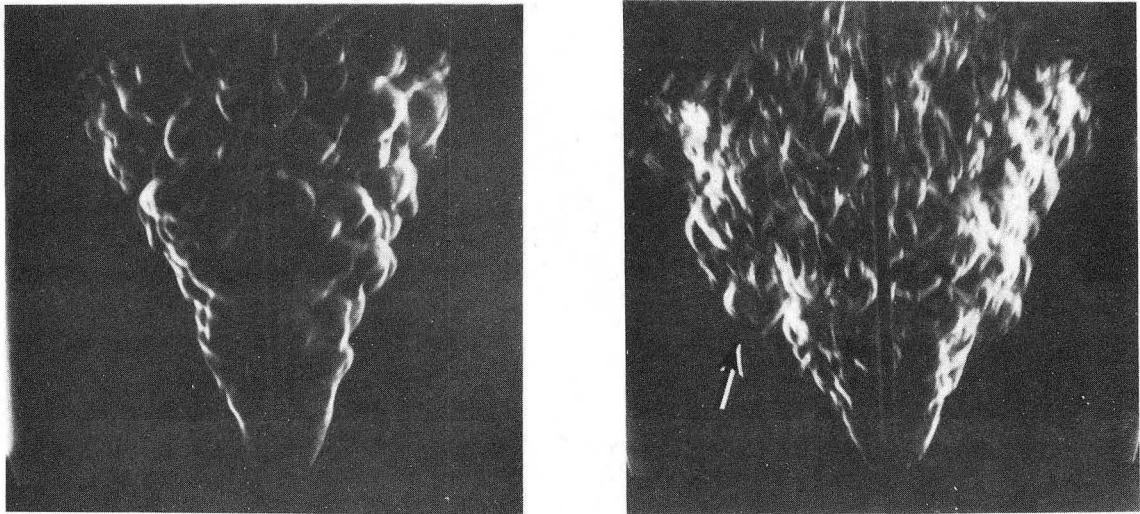
Fig. 4 Two dimensional velocity vector fields of three flames using (a) the grid, (b) plate #1, and (c) plate #2 to generate incident turbulence, $U_{\infty} = 7.0$ m/s, $\phi = 0.75$, ----- mean flame position, cold boundary.



(a)

(b)

Fig. 5 Schlieren records of two V-shaped turbulent flame with $U_{\infty} = 7.0$ m/s, $\phi = 0.75$ using: (a) the grid and (b) plate #1 to produce incident turbulence.



(a)

(b)

XBB 817-6369A

Fig. 6 Schlieren records of two conical turbulent flame with $U_{\infty} = 7.0$ m/s, $\phi = 0.75$ using: (a) the grid and (b) plate #1 to produce incident turbulence.

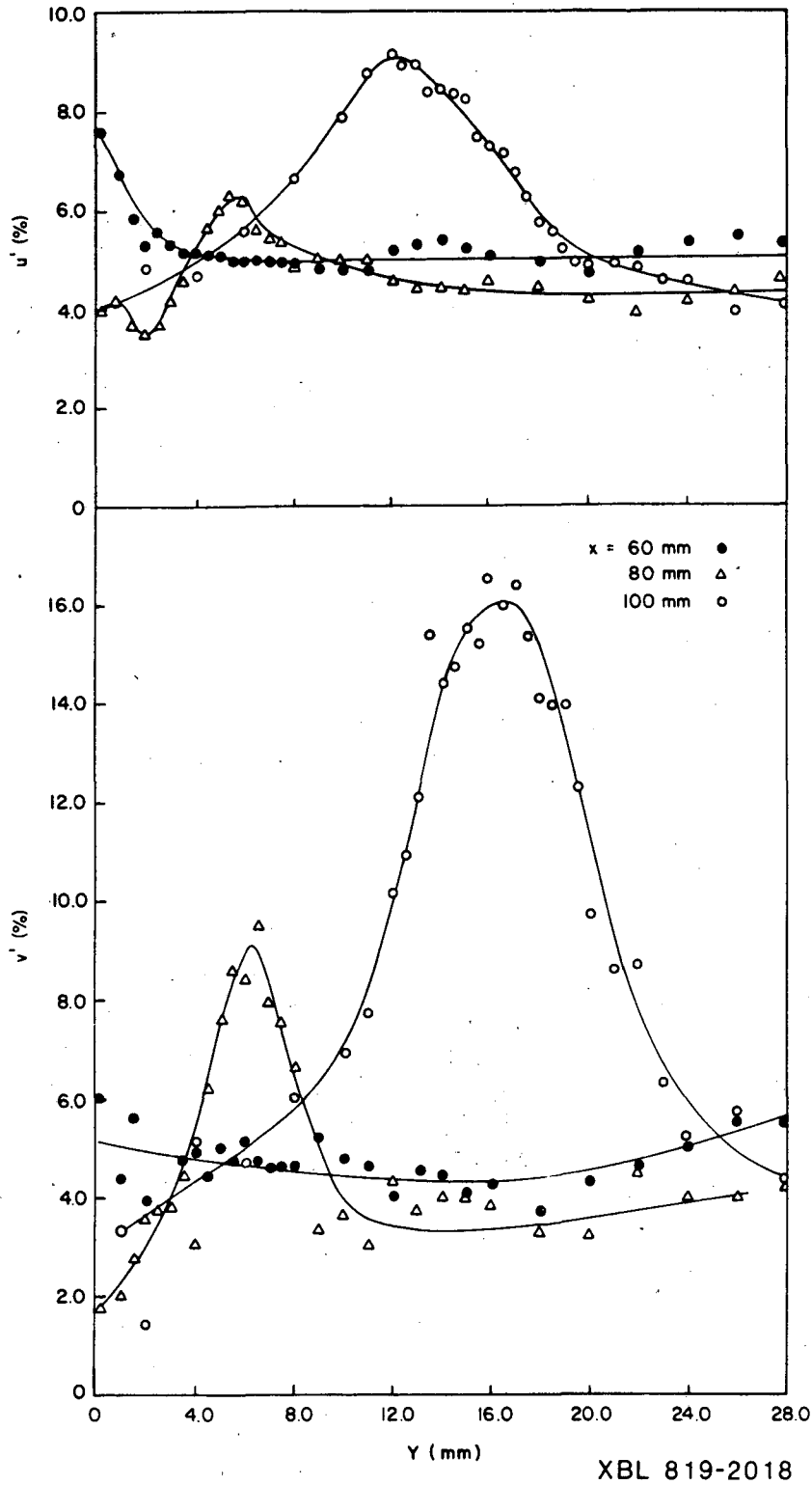
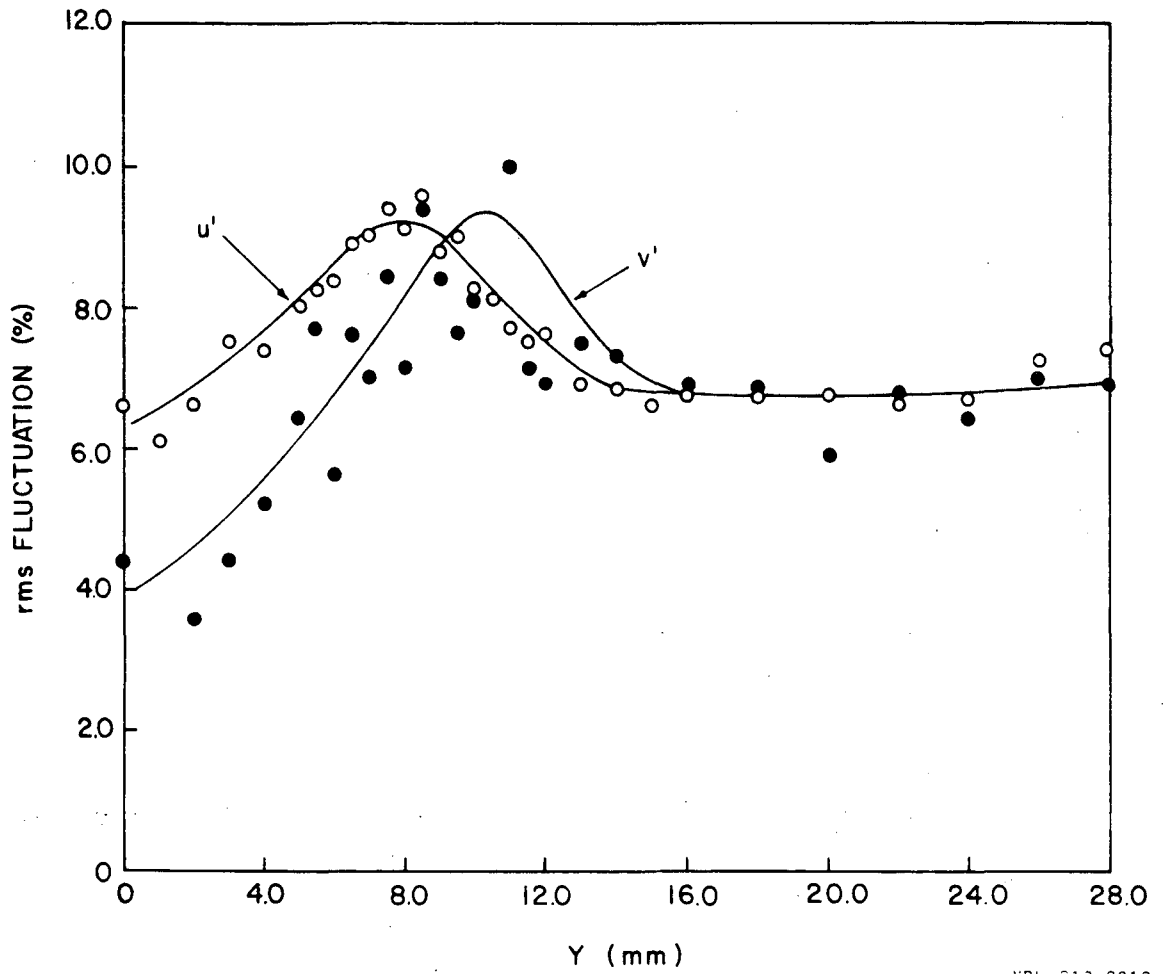
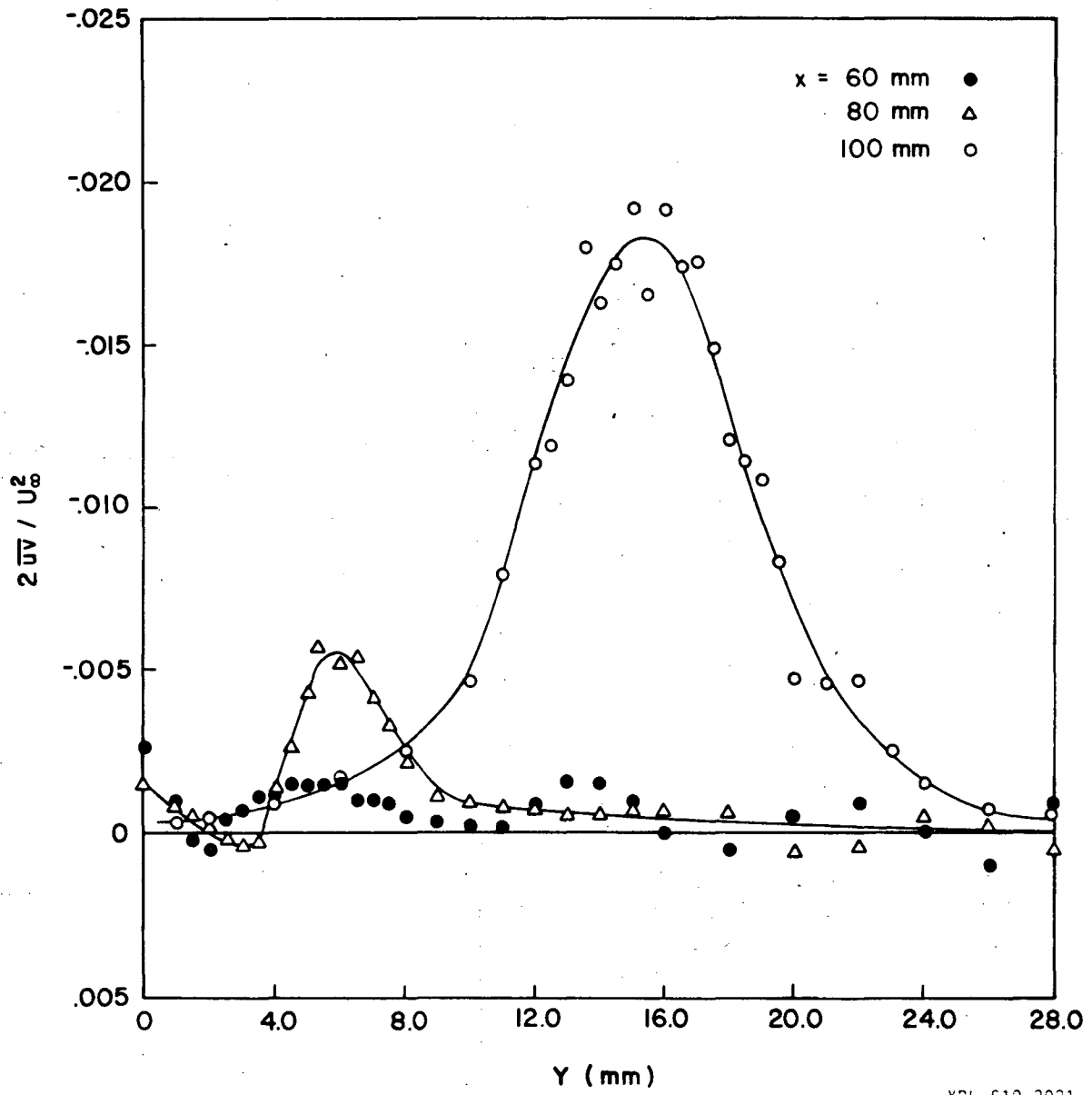


Fig. 7 Rms fluctuation profiles for $U_{\infty} = 7.0$ m/s
 $\phi = 0.75$ with grid induced incident
turbulence.



XBL 819-2019

Fig. 8 Rms fluctuation profiles at $x = 80$ mm for $U_{\infty} = 7.0$ m/s, $\phi = 0.75$ with incident turbulence induced by plate # 1.



XBL 819-2021

Fig. 9 Reynolds stress profiles for $U_\infty = 7.0$ m/s, $\phi = 0.75$ with grid induced incident turbulence.

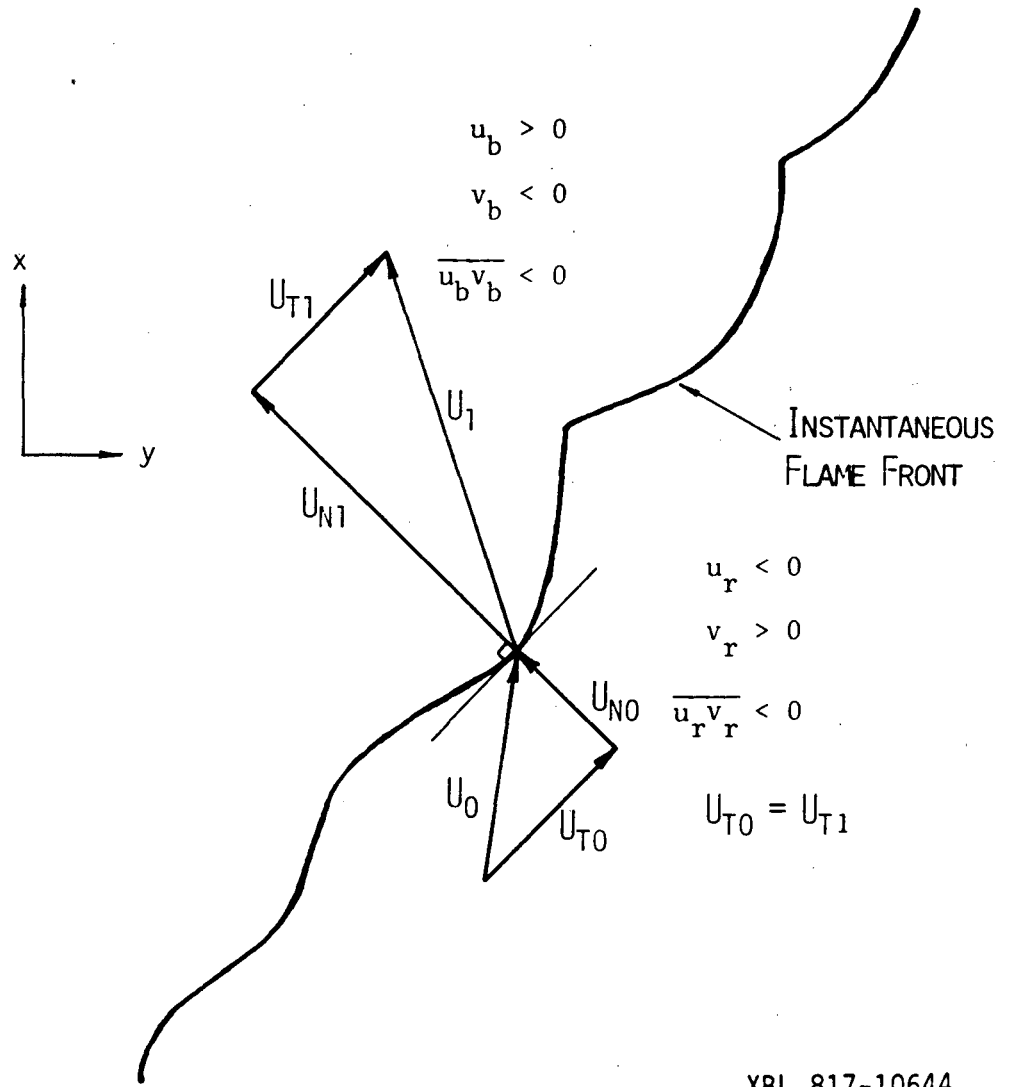


Fig. 10 Interaction of flow with convoluted flame fronts.

XBL 817-10644

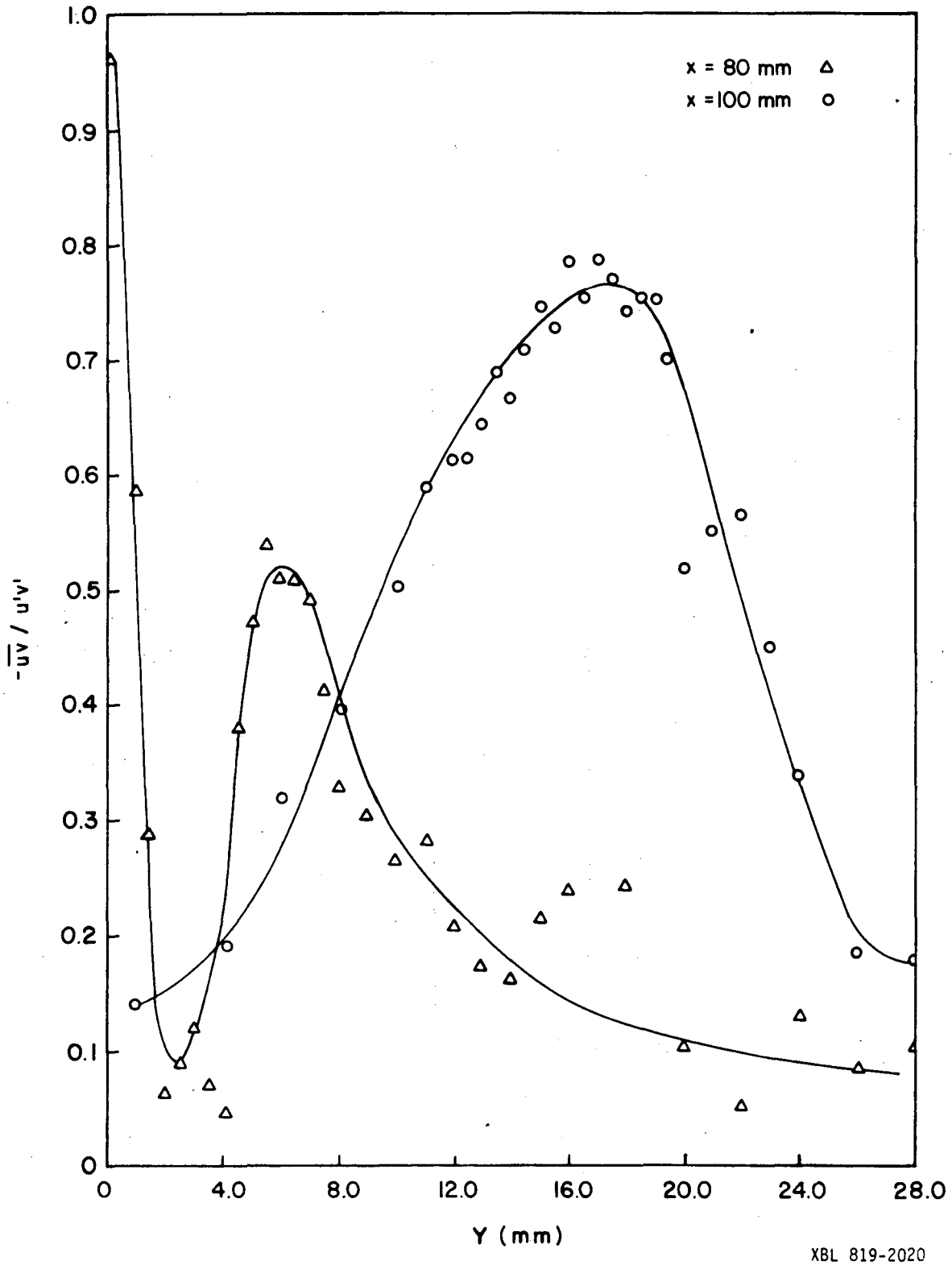
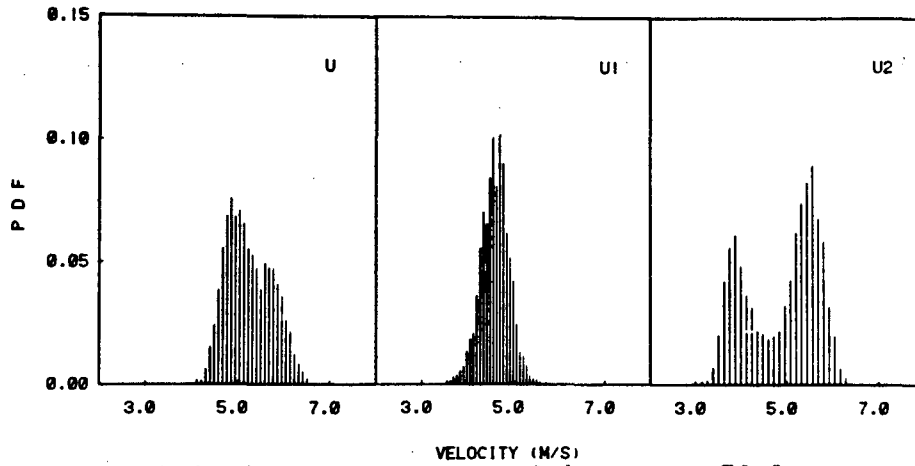
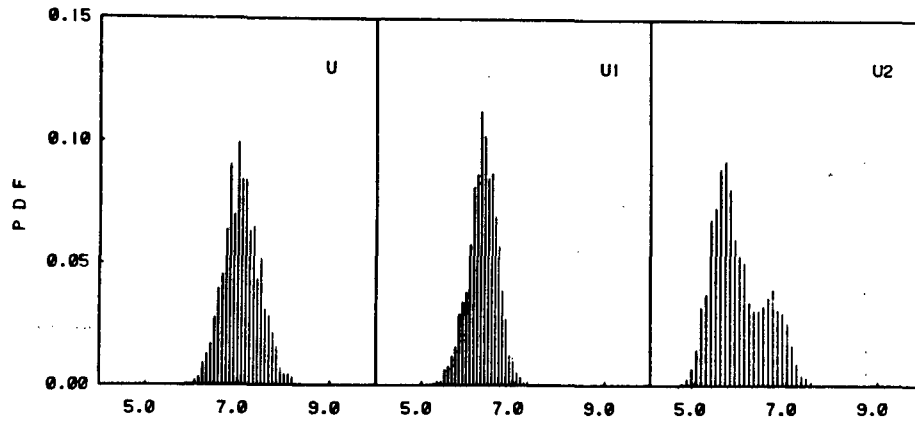


Fig. 11 Coefficient of correlation ($-\overline{u'v'}$ / $u'v'$) profiles for $U_{\infty} = 7.0$ m/s, $\phi = 0.75$ with grid induced incident turbulence

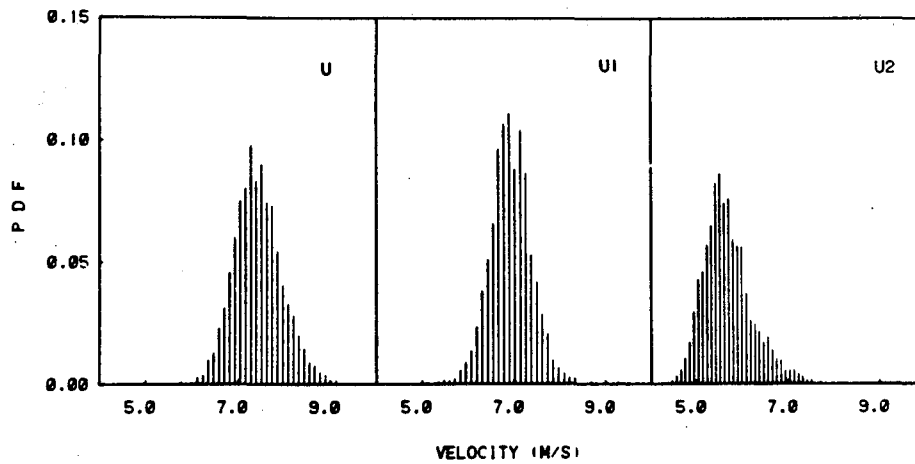
XBL 819-2020



a. $U_{\infty} = 5.0$ m/s, $\phi = 0.8$, $y = 6.0$ mm, $x = 70.0$ mm
with grid induced turbulence



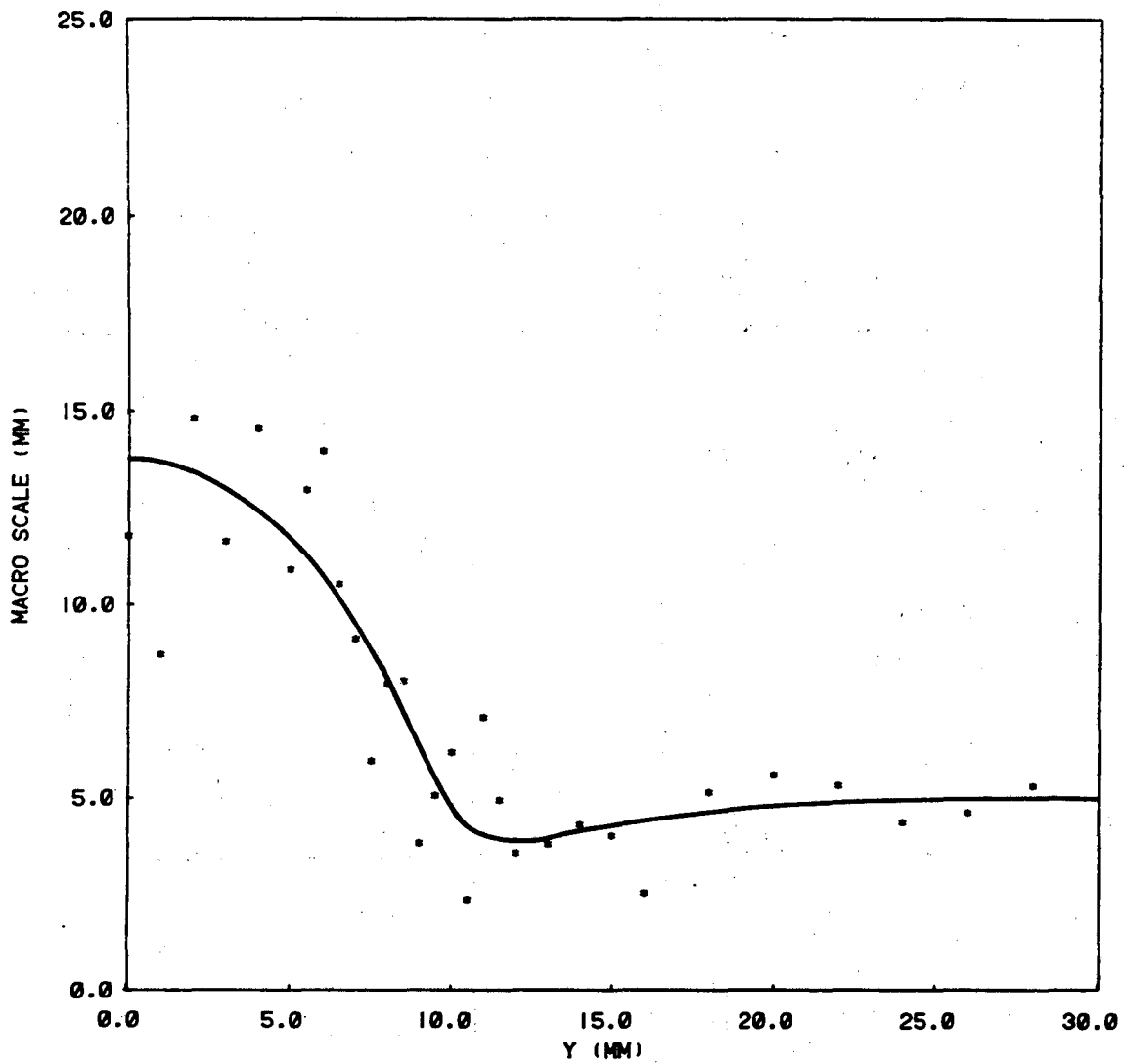
b. $U_{\infty} = 7.0$ m/s, $\phi = 0.75$, $y = 6.5$ mm, $x = 80.0$ mm
with grid induced turbulence



XBL 819-4932

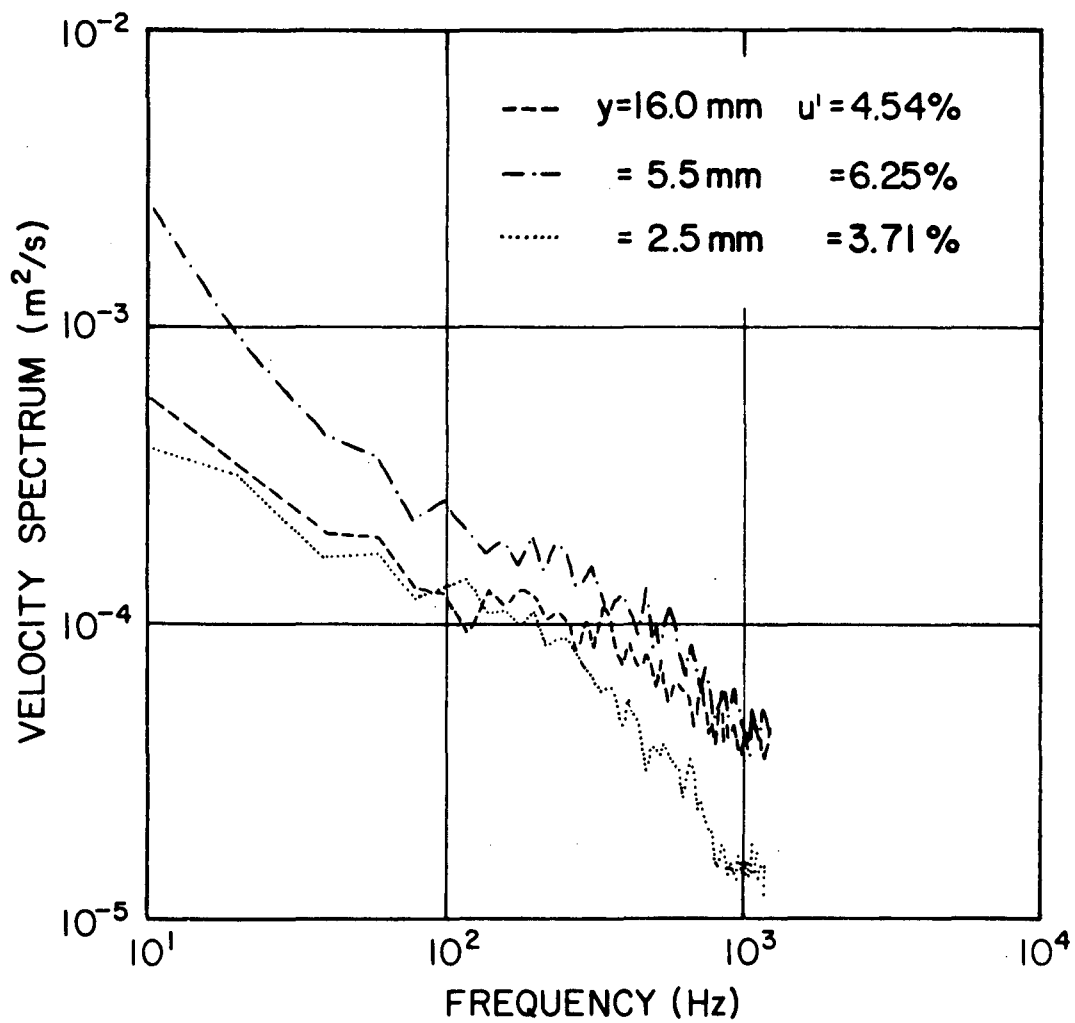
c. $U_{\infty} = 7.0$ m/s, $\phi = 0.75$, $y = 12.0$ mm, $x = 90$ mm
with perforated plate #1 induced turbulence

Fig. 12 Probability density functions



XBL 819-4931

Fig. 13 Macroscale profile for $U_{\infty} = 7.0$ m/s, $\phi = 0.75$ at $x = 90$ mm with perforated plate (#1) induced turbulence.



XBL 819-2064

Fig. 14 Spectral density distribution for $U_{\infty} = 7.0$ m/s, $\phi = 0.75$ at $x = 80$ mm with grid induced incident turbulence.

This report was done with support from the Department of Energy. Any conclusions or opinions expressed in this report represent solely those of the author(s) and not necessarily those of The Regents of the University of California, the Lawrence Berkeley Laboratory or the Department of Energy.

Reference to a company or product name does not imply approval or recommendation of the product by the University of California or the U.S. Department of Energy to the exclusion of others that may be suitable.

TECHNICAL INFORMATION DEPARTMENT
LAWRENCE BERKELEY LABORATORY
UNIVERSITY OF CALIFORNIA
BERKELEY, CALIFORNIA 94720